Laser Diagnostics of Reacting Stagnation Point Flow

C. J. Posillico* and S. Lederman†
Polytechnic University, Farmingdale, New York

Raman spectroscopy techniques are used to determine the properties of the oxidation of methane in premixed stagnation flow at atmospheric pressure via temperature and N_2, O_2, and CO_2 concentration measurements. Simultaneous velocity measurements also are made in the flowfield by applying laser Doppler velocimetry. The resulting data include plate-stabilized as well as nozzle-stabilized modes of reaction taken over a range of concentrations of methane and mass flow rates in the impinging stream. Comparisons are made to similar measurements made in the corresponding free jet structures. The data include approximations of the heat transfer to the stagnation surface. The effects of flame stretch and preferential diffusion, as observed previously in other reaction problems, exist and can be clearly pinpointed. Measurements made in cold, premixed CH_4-air-CO_2 jets and their corresponding reacting mode are used to corroborate the above measurements. The small width of the quench layer adjacent to the stagnation surface, the cool temperatures prevalent in the immediate stagnation region, and the existence of "ring" flame structures in the plate-stabilized case have also been established. Experiments of this type, coupled with theoretical predictions, provide insight into kinetics of combustion reactions when flow strain, convection, and diffusion processes are prevalent.

Nomenclature

c	= velocity of light
C	= calibration constant
D	= jet diameter
F/A	= fuel-to-air ratio
$G_0(v)$	= vibrational energy states referred to $v = 0$ level, cm^{-1}
h	= Planck's constant
H	= nozzle-plate distance
I_{as}	= anti-Stokes scattered signal intensity
I_0	= incident laser intensity
I_S	= Stokes scattered signal intensity
k	= Boltzmann constant
Le_c	= critical Lewis number value
N	= specie concentration
R	= jet radius
v	= vibrational quantum number, = 0,1,2,3,...
w_r	= radial velocity component
w_D	= nozzle exit velocity
w_z, wz	= normal velocity component
z	= plate coordinate
z'	= nozzle coordinate
α'	= derivative of the polarizability tensor in the isotropic sense
ϵ	= relative strain rate parameter, = $w_D/18.6$
γ'	= derivative of the polarizability tensor in the anisotropic sense
ν	= wave number of molecular specie's Raman vibrational shift, cm^{-1}
ν_0	= wave number of input laser radiation
ϕ	= equivalence ratio

Introduction

IN this work, modern diagnostic techniques associated with scattering of incident laser light are used for significant flow measurements. One deals with the inelastic spontaneous scattering as the basis of the Raman diagnostic technique.[1] The other deals with the Doppler shift of scattered coherent light from small seed particles in the flowfield.[1]

Both methods have advantages over physical measuring probes. The more important ones to note are: reliable measurements made at a point affording good spatial resolution, nonintrusive measurements that prevent disturbance in the particular region or field under observation, and fast response time and accessibility into experimental situations that are not possible by physical probes because of either geometric constraints or environmental tolerance. These advantages are especially important when considering the geometry and lack of meaningful experimental data pertaining to the present flow system.

The goal of this paper is to use both techniques indicated above in determining a reacting flame/jet stagnation point flowfield and its properties. The concentration, temperature, and velocity are some of the most important variables that, in conjunction with other derived parameters, may be used to completely describe the stagnation point flowfield. In general, it is hoped that the reduced data will be useful in modeling similar physical setups such as rocket motors or combustion chambers. In particular, the development of near-lean-limit engines (in response to emission standards and fuel costs) will require additional studies of flame/wall interaction. The lower temperature and pressure characteristics of these engines cause emission of undesirable toxic products via thickened quench layers formed adjacent to the cylinder walls under off-stoichiometric operation.[2] In addition, as the mixture strength is made leaner, starting from approximately stoichiometric value, variations in combustion from cycle to cycle increase, and eventually misfiring occurs in some cycles. These variations have been linked to effects of flowfield strain on the reaction process.[2] In both cases above, the present work should help investigate the nature of these effects.

Theoretical Presentation

Spontaneous Raman Theory/Laser Doppler Theory

Since Raman scattering theory and laser Doppler theory pertaining to flow measurements are well documented in Refs. 1, 3, and 4, only the basic governing equations concerning specie concentration and temperature and velocity measurements will be presented.

The concentration of a given specie in a mixture may be obtained from the intensity of the vibrational Stokes or anti-Stokes line of the scattered laser energy due to the specie of interest as done in the present case. It can be shown using the

Received Sept. 25, 1986; revision received Feb. 13, 1988.

*Senior Research Associate, Department of Mechanical and Aerospace Engineering; currently, Senior Research Scientist, General Applied Science Laboratories, Ronkonkoma, NY. Member AIAA.

†Professor, Department of Mechanical and Aerospace Engineering. Member AIAA.

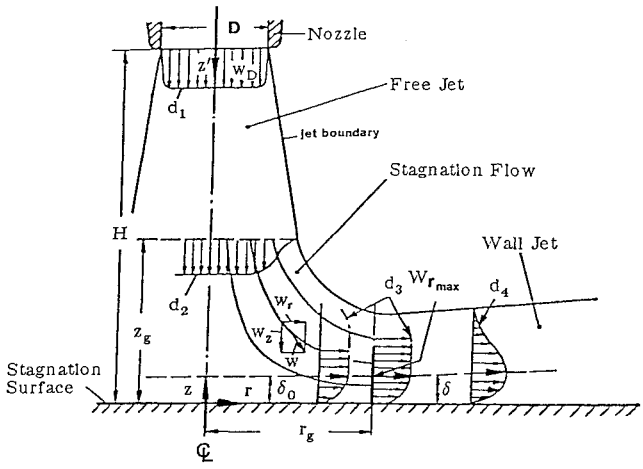

Fig. 1 Schematic flowfield of impinging jet.[8]

polarizability theory of Placzek that the scattered intensity of the vibrational lines for individual species can be written as[3]

$$(I_{s,as}/I_0) = CN(\nu_0 \pm \nu)^4 f(\alpha',\gamma') \tag{1}$$

The distribution of the molecules over the different quantum states in thermal equilibrium is given by the Maxwell-Boltzmann relation, where the number of molecules in each of the vibrational states is approximated by[3]

$$N_v = N \exp[-G_0(v)hc/kT] \tag{2}$$

Due to the short laser pulse duration (10–15 ns), we may assume local thermodynamic equilibrium and therefore, for a given specie sample, applying Eq. (1) in conjunction with Eq. (2) results in

$$\frac{I_s}{I_{as}} = \frac{(\nu_0 - \nu)^4}{(\nu_0 + \nu)^4} \exp\left(\frac{hc\nu}{kT}\right) \tag{3}$$

Equations (1) and (3) are sufficient to obtain both the number density and the temperature of any molecular species in a gas via simultaneous measurements of I_s and I_{as}. An important point to be observed is that the scattered intensity is proportional to the fourth power of the frequency (making the choice of the laser source a noteworthy factor).[5]

The laser Doppler velocimeter (LDV) employs the shift in frequency (the Doppler shift) of light that is scattered from a moving object. The shift in frequency depends on the velocity of the scattering surface.

The present optical mixing method allows measurement of a frequency-modulated signal and is often conveniently interpreted as arising from light scattered by the flow tracing particles as they pass through the interference fringes found in the measuring volume at the intersection of two incident monochromatic beams.

If a flow tracing particle with velocity V is passing through this system of fringes with spacing X in a normal direction to the fringes, then the scattered light would appear to fluctuate with a measurable angular frequency of

$$\omega_D = (2\pi V/X) \tag{4}$$

Impinging Jet Theory

Previous experimental work on reacting impinging jets[6] has shown that reacting and nonreacting (heated) wall jets can have similar parameter profiles. Nonreacting impinging jets (Fig. 1) therefore will yield insight into the basic hydrodynamic structure of the present flowfield. The three characteristic regions are: the free jet region (d_1), the stagnation flow region (r_g, z_g, d_2), and the region of radial flow outside the stagnation zone (d_4), also called the wall jet region after the theoretical work of Glauert.[7]

Martin[8] reports empirical adjustments to the ideal stagnation flow boundary layer equation for jets of finite width as

$$\frac{\delta_0}{D} = \left(\frac{1.95}{Re^{1/2}}\right)\left(1.04 - 0.034\frac{H}{D}\right)^{-1/2} \tag{5}$$

For typical Reynolds numbers (say, of the order of magnitude of 10^4 or higher) the boundary-layer thickness δ_0 in the stagnation zone will reach about 1/100th of the nozzle diameter.

One condition on the derivation of the wall jet solution was that the static pressure on the surface be constant everywhere and be equal to the ambient pressure. Experimental data have shown[9] that surface static pressure is quite uniform for radial positions up to about one jet radius and then rapidly drops to the ambient static pressure at about two jet radii. This suggests that the wall jet theory would be applicable at or about the radial position $r/R \approx 2$ and that stagnation flow is a good approximation up to the range of radial positions $r/R \approx$ 1–1.50. These values appear to be of the same order as those reported by Milson and Chigier[6] for a reacting wall jet and will be a guide for evaluating data in the present case.

Reacting Flow Analysis

Unlike the present approach, the majority of analytical solutions for impinging-type flows deal solely with thin uniform flame structures in simple shear and straining flows; in the case of impinging jets, usually the linear ideal stagnation flow is encountered with such a flame structure.[10,11] In general, most numerical analysis in the literature deals with simple, one-dimensional, thin-flame propagation near or against a cold boundary.[12] Similar experimental analysis of the present impinging configuration[6,13] has not treated the problem to the degree presently undertaken. It is the aim of the present analysis to apply some of the more generalized theoretical features found in the literature to an actual impinging flame to make some correlations via experimental data and observations.

Flame propagation is strongly influenced by the effects of strain in the flowfield. It is clear that hydrodynamic strain can be correlated to changes in the flame surface area and local burning velocity. One of the first to study flame area variation with strain was Karlovitz et al.[14] in 1953. Since then, there has been much interest in the relationship between strain in the form of flowfield velocity gradients and the local burning velocity or reaction rates. Most of the important aspects of the effects of strain on flame structure have been summarized by Law,[10] who points out that flame behavior, in particular its temperature, depends on the relative rates of heat and mass diffusion or whether $Le > 1$ or < 1. For $Le = 1$, heat loss and mass gain occurred at the same rate in such a way that the flame temperature is the defined adiabatic flame temperature T_{ad}. However, for $Le \gtrless 1$ or $Le \gtrless Le_c$, the reaction might proceed in such a manner that $T_{flame} \lesseqgtr T_{ad}$ due to preferential diffusion caused by the flame stretch effects resulting from the imposed velocity gradient. Changes in reaction residence time, represented by the Damköhler number Da produce similar results. Sato and Tsuji[15] have calculated the temperature response for this particular geometry with Le as a parameter as shown in Fig. 2a. Note for $Le < Le_c$, T_{flame} produces a local maximum. It is the object of this work to point out some straining effects on reaction behavior in the free-jet, stagnation flow, and wall-jet zones and any interrelationships among these zones.

Experimental Apparatus

Raman data and LDV data were taken simultaneously during the course of the entire experiment. The Raman/LDV system is shown in Fig. 3; performance and design details can be found in Ref. 16.

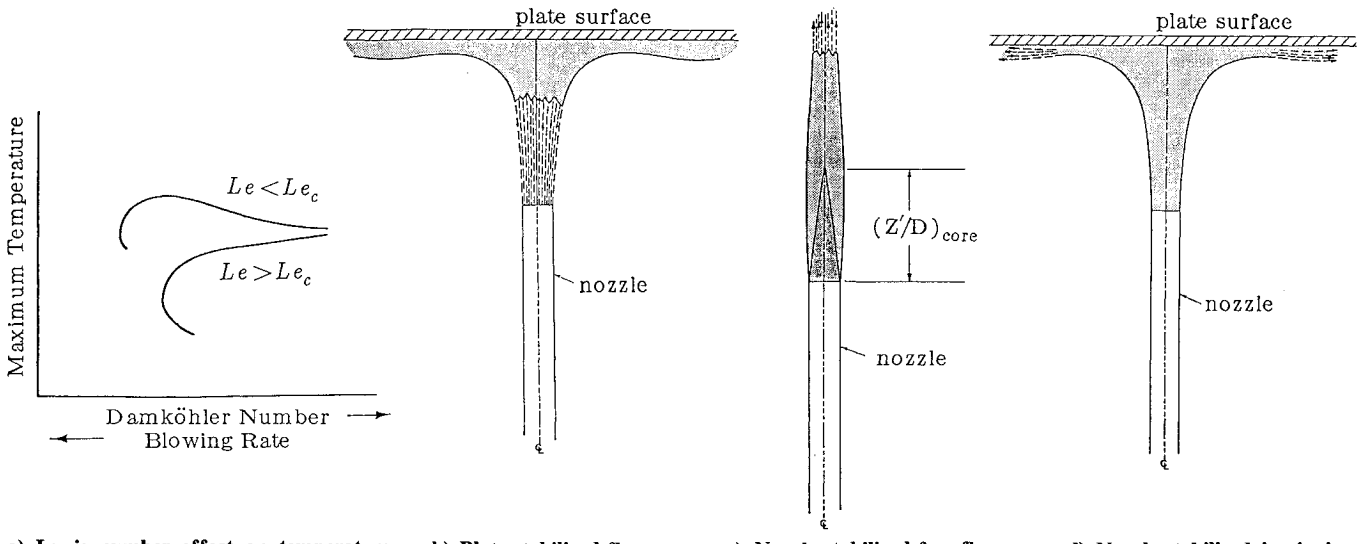

a) Lewis number effect on temperature response[15] **b) Plate-stabilized flame** **c) Nozzle-stabilized free flame** **d) Nozzle-stabilized impinging flame**

Fig. 2 Flame structure vs temperature response.

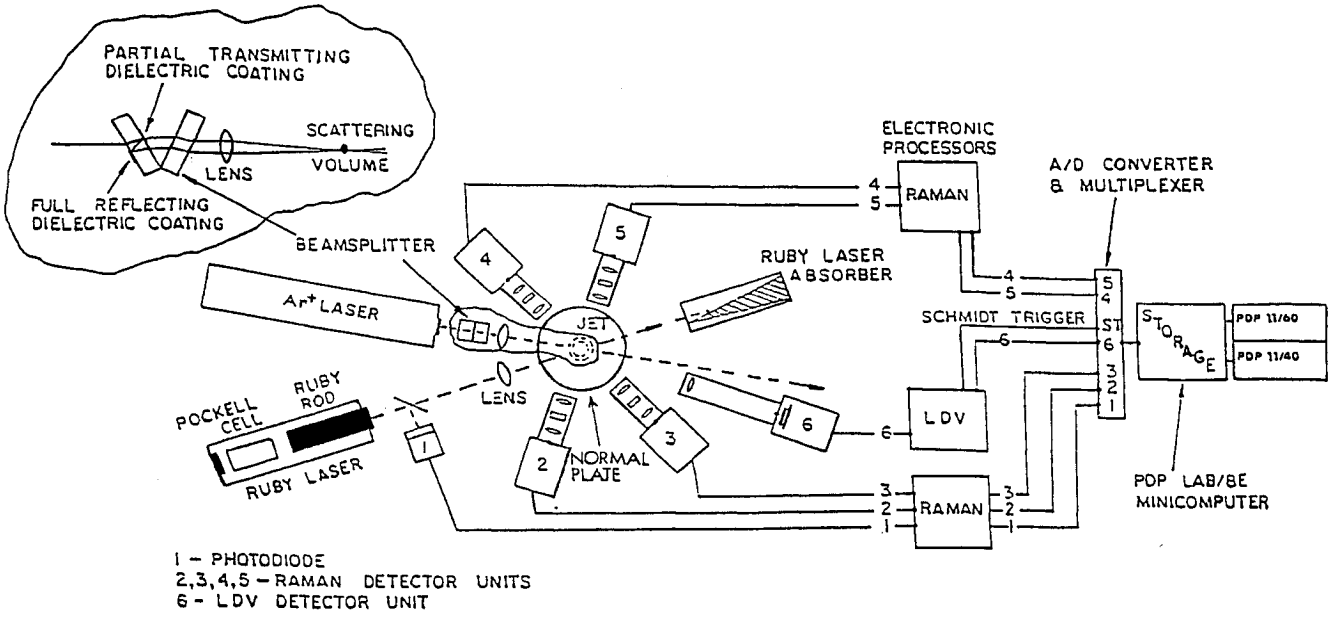

Fig. 3 Integrated four-component Raman one-dimensional LDV measurement system schematic.

Raman/LDV System

The incident source was a high-power 150 MW, 3 J, Q-switched, 10–20 ns pulse, 6943 Å vertically polarized ruby laser. The maximum repetition rate was 60 pulses/min. The physical beam diameter was ~ ½ in. Each plotted flame position represents 300 statistically filtered data samples. Temperature and concentration accuracy is better than 5%.

The incident beam was focused down via special optical arrangements[16] to increase the photon flux per square centimeter (yielding a higher signal-to-noise ratio) as well as to reduce the physical beam size in the measuring volume permitting measurements in closer proximity to solid surfaces and yielding spatial resolution of 1 mm.

For the LDV system, the incident source was an 8 W maximum power, continuous wave, 5145 Å Ar^+ laser. The LDV operated in the dual-beam differential scatter mode[4] and was a one-component system measuring velocity in the convective flow direction, i.e., the w_z component of the velocity vector.

The electronic detection system consisted of an operational amplifier and discriminator, as well as a signal processor system designed at this laboratory. The photomultiplier tube output was of the form of a modulated sine wave, the frequency of which was proportional to the particle velocity.[16] Each velocity data point in this work represents 500 statistically treated data samples. Accuracy for velocity data is better than 1%.

Flow and Wall System

The system is set up so that any combination of CH_4 and air and CO_2 can be mixed and introduced into the jet. Provisions have been made to adjust the Al_2O_3 seed particles for the LDV to optimize the seeding rate for various levels of mass flows for both the air and CH_4 flow lines. This allowed for efficient seeding at leaner or richer flows at various jet velocities. The jet diameter here was 10 mm.

The cooled wall apparatus was constructed of two pieces of jig-plate aluminum allowing the shell to "breathe" while being heated. The heat-transfer rate $\dot{Q}$ (and, thus, the surface temperature) was simply controlled by regulating the flow of cool tap water through the shell.

Experimental Results

Flame-Wall Heat Transfer

The flow rate of water through the cooled plate was 1.25 gal/min. The difference between the input and output cooling water was measured and used to calculate the heat transfer to the plate.

Heat transfer to the wall from the flame through convection and radiation is given by

$$Q_{cr} = \dot{m}_{H_2O} \cdot (C_p)_{ave_{H_2O}} \cdot \Delta T_{H_2O}$$

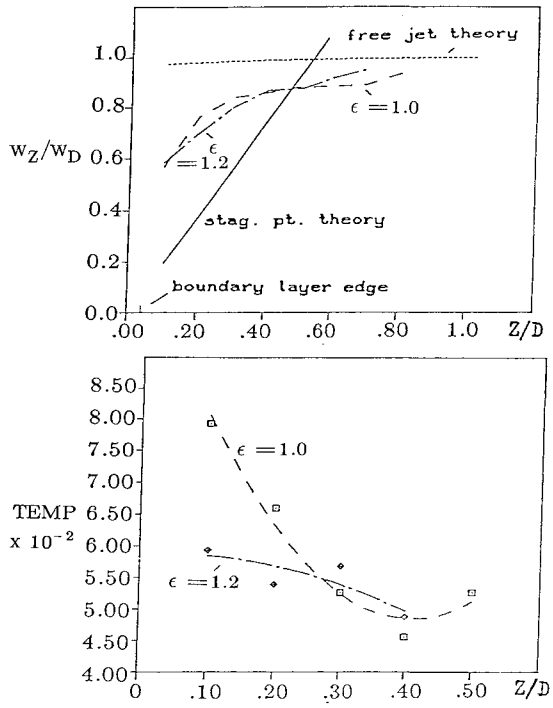

Fig. 4 Plate-stabilized flame: centerline temperature and axial velocity profiles, $H/D = 3.1$.

We can compare Q_{cr} with the average total heat-transfer rate computed from Milson and Chigier who used a reacting flame resembling the present jet setup. This value, 31,113 Btu/h, is roughly 2.5 times the value of Q_{cr} above. However, their nozzle Reynolds number is 7000, while the typical nozzle Reynolds number value for the present impinging jets is 3100 or approximately 2.5 times lower in value. Milson and Chigier reported elevated heat-transfer rates and coefficients with increasing nozzle Reynolds number, and it is clear that there is a direct correlation between flow parameters at the nozzle and the resulting heat-transfer mechanism at the flame-boundary interface.

Unless otherwise noted, the plotted data to follow will be presented as radial profiles with r/R as the radial abscissa, and all data is curve-fitted via a least-squares regression analysis[16] using a numerical program that computes the coefficients of all possible polynomial curves between the powers of 1 and 8 and chooses the most appropriate curve based on the optimum standard deviation values computed for each polynomial. For certain plots with multiple profiles, the data points have been eliminated for clarity. The curves are only to be used as guides to help interpret the data. All data collected was from premixed CH_4-air or CH_4-air-CO_2 flames and cold jets.

All N_2 and O_2 concentration values were normalized with respect to their ambient, quiescent, and nonreacting values existing at the time data was taken. The CO_2 concentration values were normalized with respect to the value measured in a cold pure CO_2 jet at the nozzle exit at ambient conditions. This value corresponds to the same mass flow rate of CO_2 (0.0036415 lbm/s) used in the jets analyzed in the following data. This value was measured to be 6.68×10^{21} molecules/cm^3 or 0.11377 lbm/ft^3. The range of plate locations from the nozzle was from $z'/D = 1.1$–10.1, corresponding to $H/D = 1.1$–10.1.

In all cases, pointwise measurements are made of temperature, N_2 and O_2, and any premixed CO_2 concentrations; velocity measurements are made simultaneously with the other measurements at all points where measurable values exist. All values of temperature in the following plots are given in K $\times 10^{-3}$ and values of unnormalized velocity are in ft/s $\times 10^{-1}$ unless otherwise noted.

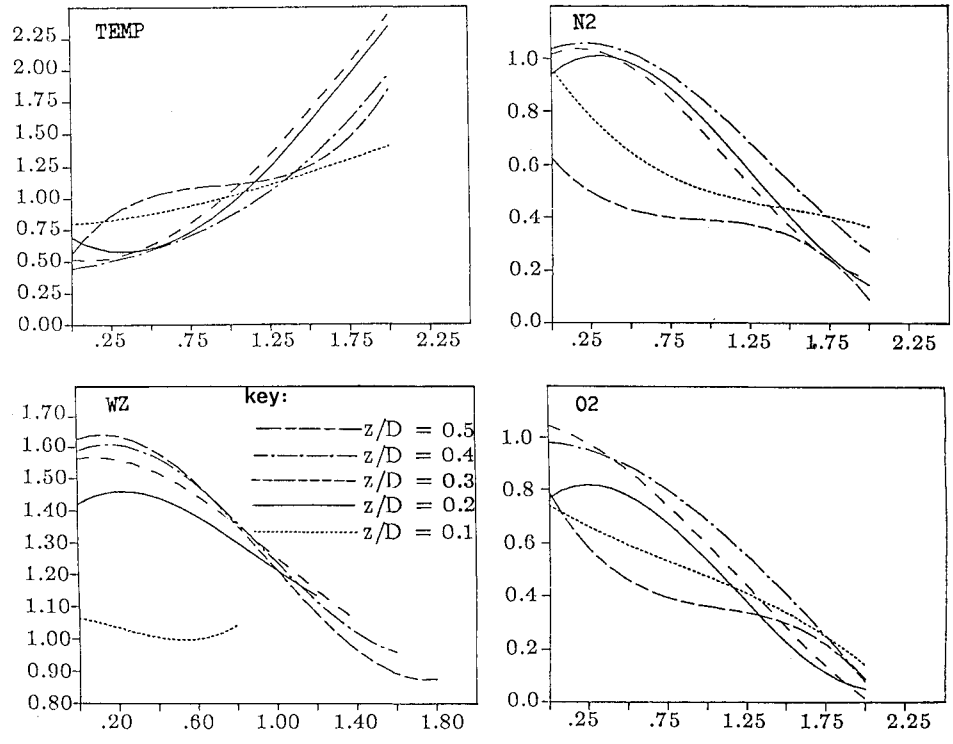

Fig. 5 Plate-stabilized flame: radial profiles at $Z/D = 0.1$–0.5, $\epsilon = 1.0$, $H/D = 3.1$.

Plate-Stabilized Flames

For the nozzle exit velocities of w_D = 18.6, 22.3, and 27.11 ft/s, the respective relative strain parameter ϵ is simply 1.0, 1.20, and 1.45. Here $F/A = 0.1857$ ($\phi = 0.67$), $H/D = 3.1$, the corresponding cold core length is approximately three-dimensional, and the flame appears visually as in Fig. 2b. In Fig. 4, the centerline axial velocity profiles normalized with respect to w_D for the cases $\epsilon = 1.0$ and 1.20 are presented, as well as cold jet stagnation point theory and cold free jet theory. The velocity remains relatively high past the stagnation line and starts to drop to zero only quite close to the plate. This delayed drop in velocity is most likely influenced by the decrease in density caused by the elevated temperatures of the reaction near the plate. This can be borne out by the corresponding centerline temperature profiles also shown in Fig. 4. The slope of axial velocity curve for $\epsilon = 1.2$ seems to have decreased somewhat, suggesting some cold jet behavior with the decreasing temperatures. The value of the cold boundary-layer thickness as calculated via Eq. (5) is approximately three times smaller than the closest data location (1 mm or $z/D = 0.1$). It is most likely that density and viscosity changes due to the reaction would cause the boundary-layer thickness to increase.

In Fig. 5, the overall flame structure for $\epsilon = 1.0$ is displayed by plotting all the temperature, velocity, N_2, and O_2 values in the vicinity of the plate together. An interesting result appears for the profiles at $z/D = 0.1$ and 0.5; $z/D = 0.1$ is the closest radial profile to the plate and one might expect cooler temperatures than at other axial positions to prevail there. This is true, except closer to the centerline of the flame, where the temperature values are higher than all other profiles except $z/D = 0.5$. A possible explanation is that the stagnation surface realistically cannot be uniformly cooled and a local "hot spot" develops around the point of impingement, thereby affecting the temperature of the fluid layers close to the plate. We also note that at $z/D = 0.5$, in the vicinity of the centerline, the temperature is higher than at all the other axial positions probed. However, at the axial positions $z/D = 0.2$–0.4, the near-centerline temperature values are somewhat below the reaction limit temperature of ~1000 K, indicating that the quench zone near the centerline extends approximately 4 mm away from the stagnation surface. Thus, it would seem that the quench region is not uniformly thick but instead is "fatter" near the centerline, indicating a cool central unreacting region. As can be seen, the N_2 and O_2 profiles have corresponding lower density values near the regions of increased reaction. The velocity plot reveals that, possibly because of the thickness of the quench layer along the plate and the cooler temperatures near the centerline, the apparent boundary-layer effects are confined relatively close to the stagnation surface at about $z/D = 0.1$ (but still about three times thicker than the corresponding cold jet boundary layer) and quickly diminish with increasing z/D. Due to entrainment of quiescent fluid along the path between the nozzle and the plate, the axial velocity component w_z is still measurable past the radial position $r/R = 1.0$ as seen in the $z/D = 0.3$, 0.4, and 0.5 profiles. Momentum flux calculations based on the value of w_z at $r/R = 1.8$ for $z/D = 0.5$ were the same order of magnitude as those flux values calculated from an equivalent non-reacting laminar wall jet based on Glauert's theory.[7]

In Fig. 6, all the measured parameters are compared at their respective axial locations for the values of $\epsilon = 1.0$ and 1.2. The temperature profiles in Fig. 6a for both cases are similar except at axial positions closer to the stagnation surface, where the increased blowing of $\epsilon = 1.2$ appears to have cooled the local "hot spot" mentioned previously. The overall effect of increasing the value of ϵ has widened the central inner core of cool temperatures by delaying the complete reaction process until positions at larger values of r/R. The values of N_2 and O_2 diverge from each other near the plate, indicating that oxygen is still being used up in any reaction that may occur in the vicinity. It is also interesting to note in Fig. 6b that

for $z/D = 0.1$, 0.2

$$N_2(\epsilon = 1.0) < N_2(\epsilon = 1.2)$$

$$O_2(\epsilon = 1.0) < O_2(\epsilon = 1.2)$$

for $z/D = 0.3$

$$N_2(\epsilon = 1.0) \approx N_2(\epsilon = 1.2)$$

$$O_2(\epsilon = 1.0) \approx O_2(\epsilon = 1.2)$$

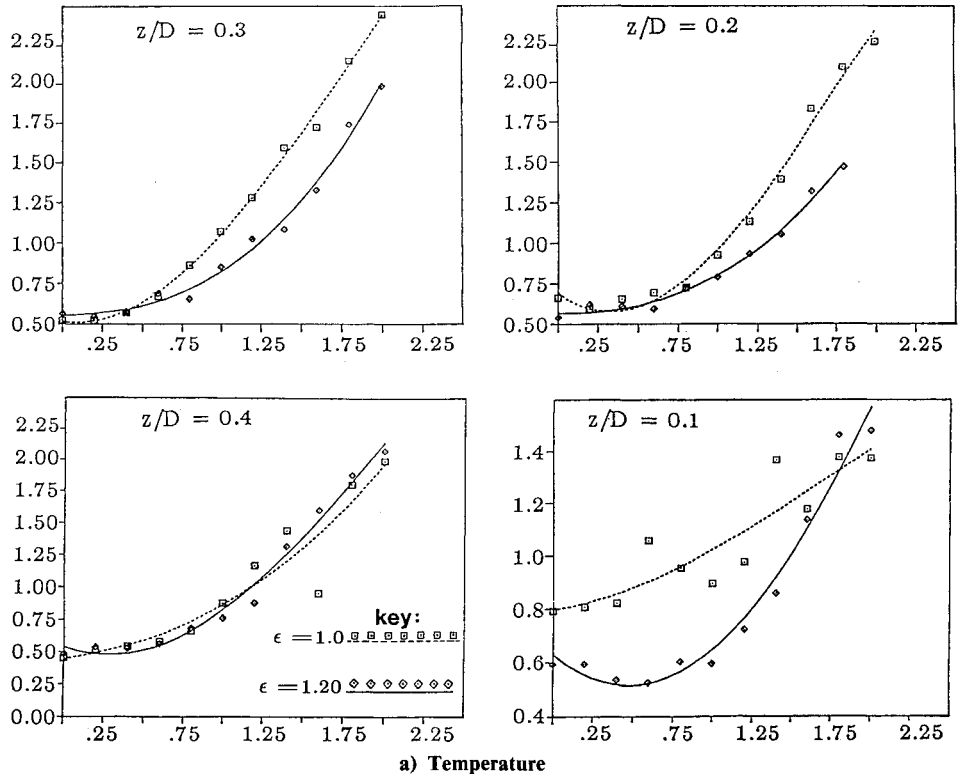

Fig. 6 Plate-stabilized flame: radial profiles at Z/D = 0.1–0.4, ϵ = 1.0 and 1.20, H/D = 3.1.

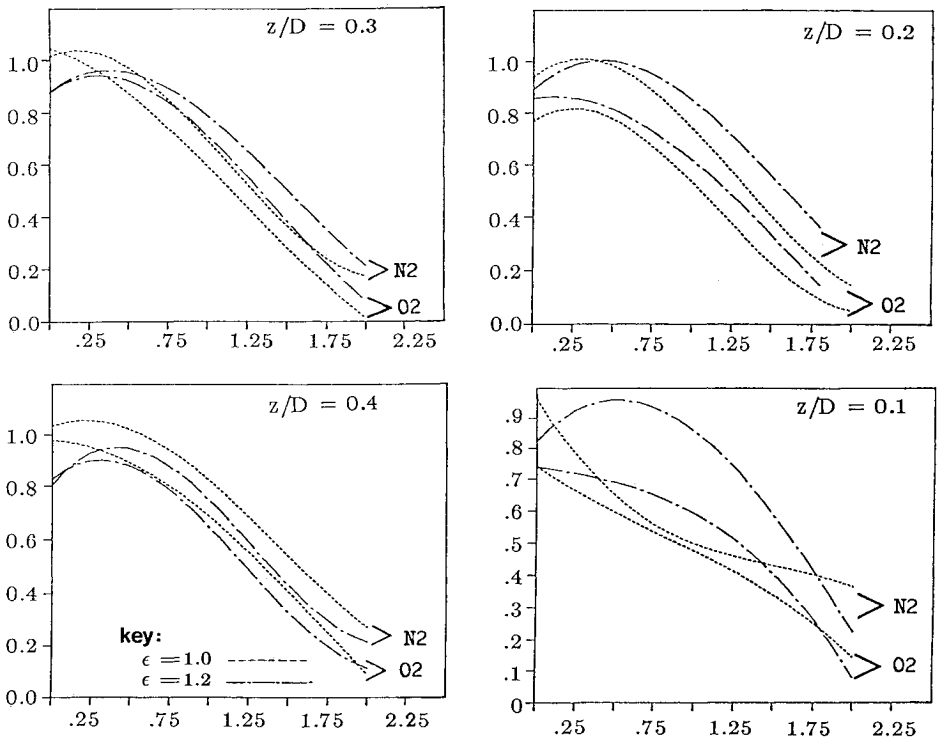

b) N_2 and O_2 normalized concentration

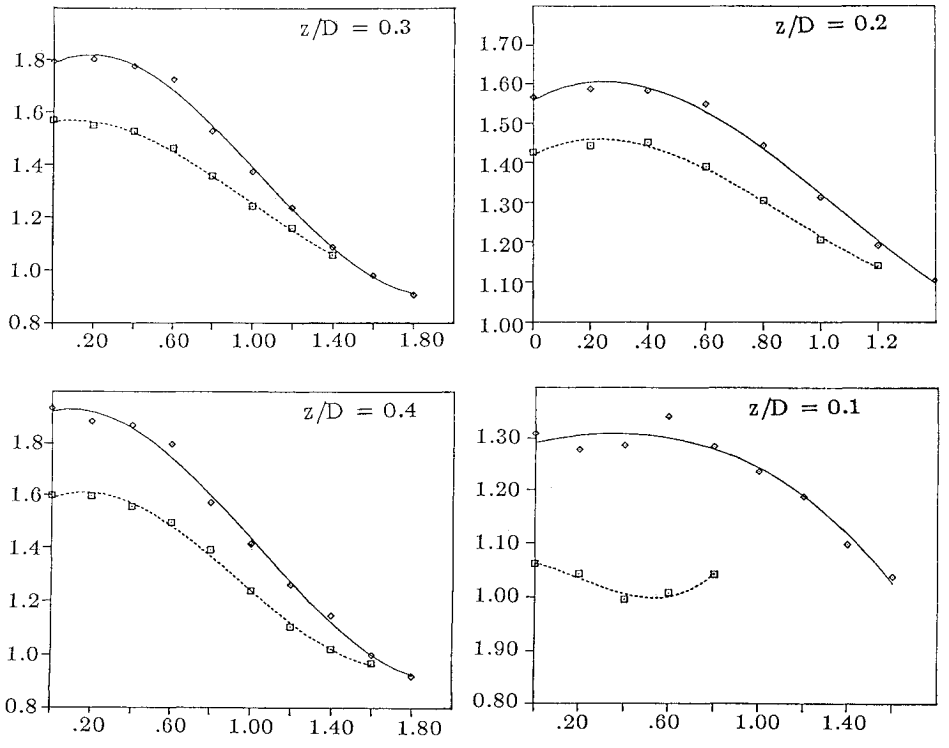

c) Axial velocity (use key of Fig. 6a)

Fig. 6 Continued; plate-stabilized flame.

for $z/D = 0.4$

$$N_2(\epsilon = 1.0) > N_2(\epsilon = 1.2)$$

$$O_2(\epsilon = 1.0) > O_2(\epsilon = 1.2)$$

This indicates that the higher strain case $\epsilon = 1.2$ yields cooler temperatures and hence higher density values close to the plate, while at about a distance of $z/D = 0.3$ from the plate the effects of the higher strain on the reaction become diminished.

As expected, the change in ϵ to 1.2 yielded higher values in the axial velocity component w_z as seen in Fig. 6c, where the results are consistent at each axial position. The w_z values for $\epsilon = 1.0$ at $z/D = 0.1$ appear to drop off more slowly than values at the other axial locations and even rose somewhat for larger values of r/R. This could be due to the higher temperature levels existing just adjacent to the hot spot existing in this particular case.

Figure 7 displays all data at $z/D = 0.1$ for the three cases $\epsilon = 1.0$, 1.2, and 1.45. It becomes quite clear in this figure that

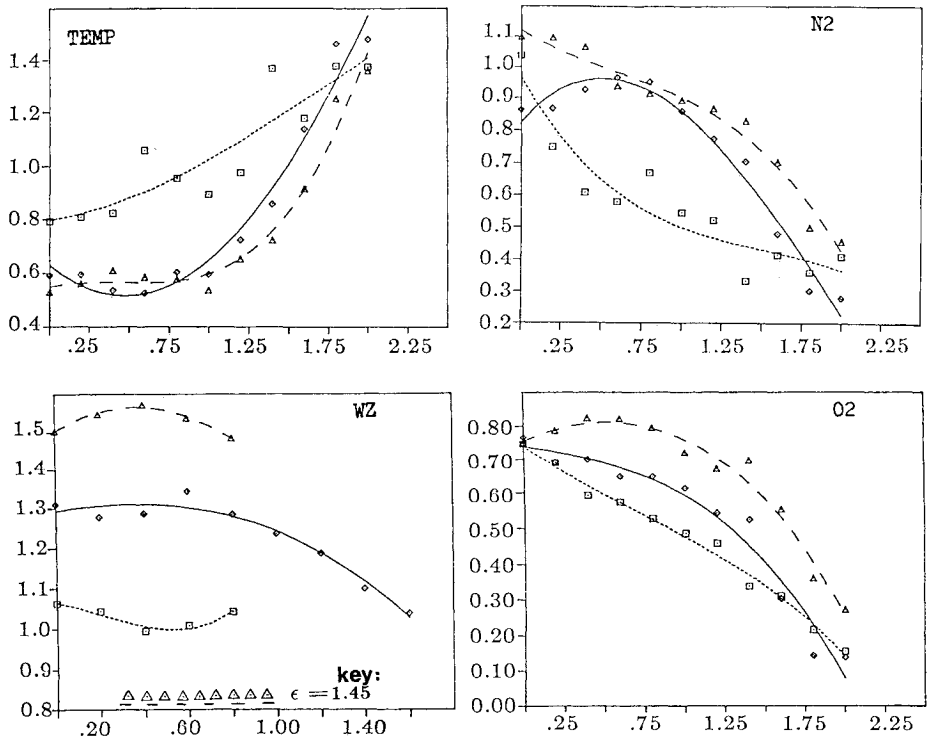

Fig. 7 Plate-stabilized flame: radial profiles at $Z/D = 0.1$; $\epsilon = 1.0$, 1.20, and 1.45; $H/D = 3.1$ (use with key from Fig. 6a).

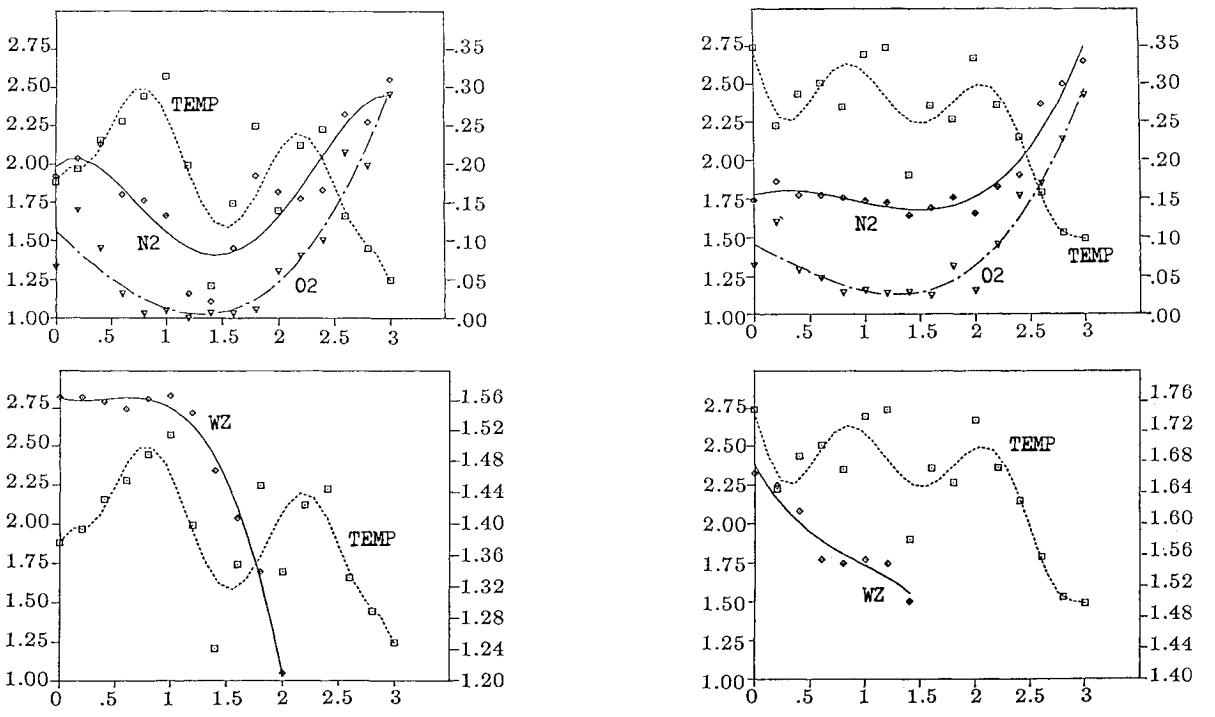

a) $Z'/D = 7.1$ (temperature is the left ordinate) **b) $Z'/D = 7.4$ (temperature is the left ordinate)**

Fig. 8 Nozzle-stabilized free flame radial profiles.

the primary effect of increasing the overall strain parameter is to widen the cool central core near the stagnation surface and to delay the reaction at larger and larger r/R positions with corresponding increases in N_2 and O_2 densities and with the resultant increases in the axial velocity component w_z.

Nozzle-Stabilized Flames

Here $w_D = 16$ ft/s and a lean flame is used with $F/A = 0.14082$ or $\phi = 0.508$ for all cases. The free flame appears visually as in Fig. 2c, and its parameters are presented in Fig. 8. These data are necessary to identify flame structure before the stagnation condition is imposed. For this particular case, $(z'/D)_{ct} \cong 7.5$; this is where the stagnation surface will be placed, as well as below the core tip at $z'/D = 1.0$ and above the core tip at $z'/D = 10.0$. Figures 8a and 8b present data in the vicinity of the core tip and the data in Fig. 8c (where the symbols for the $z'/D = 7.4$ curves have been eliminated for clarity) gives the relative differences in parameters several diameters above and below the flame core tip. The data in Fig. 8c both above and below $z'/D = 7.4$ showed no real variation

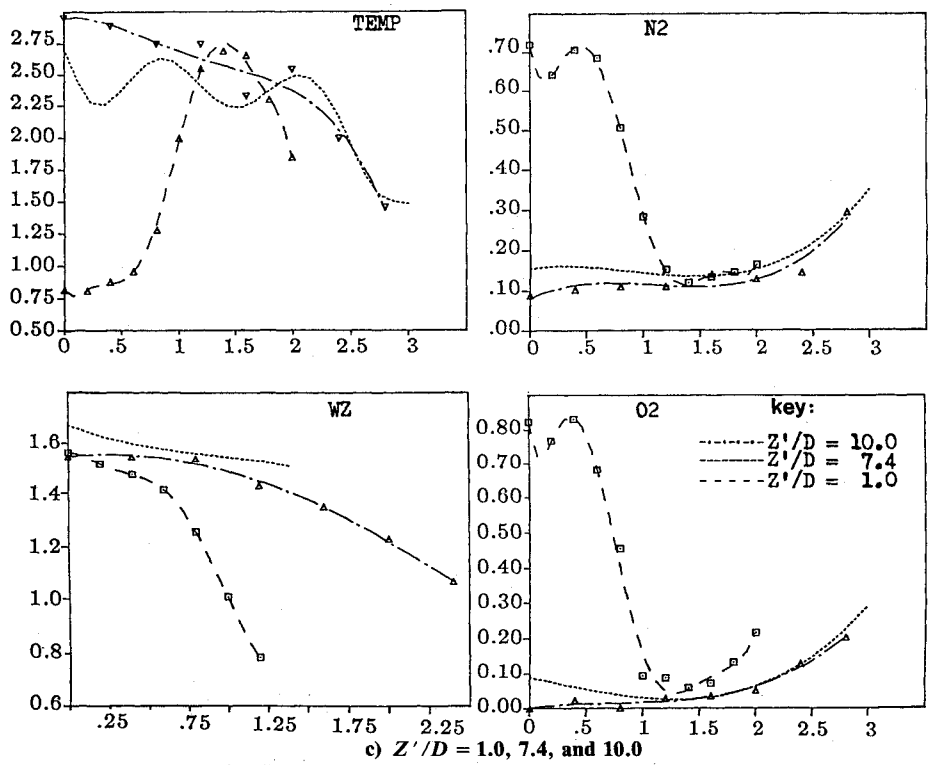

c) Z'/D = 1.0, 7.4, and 10.0

Fig. 8 Continued; nozzle-stabilized free flame radial profiles.

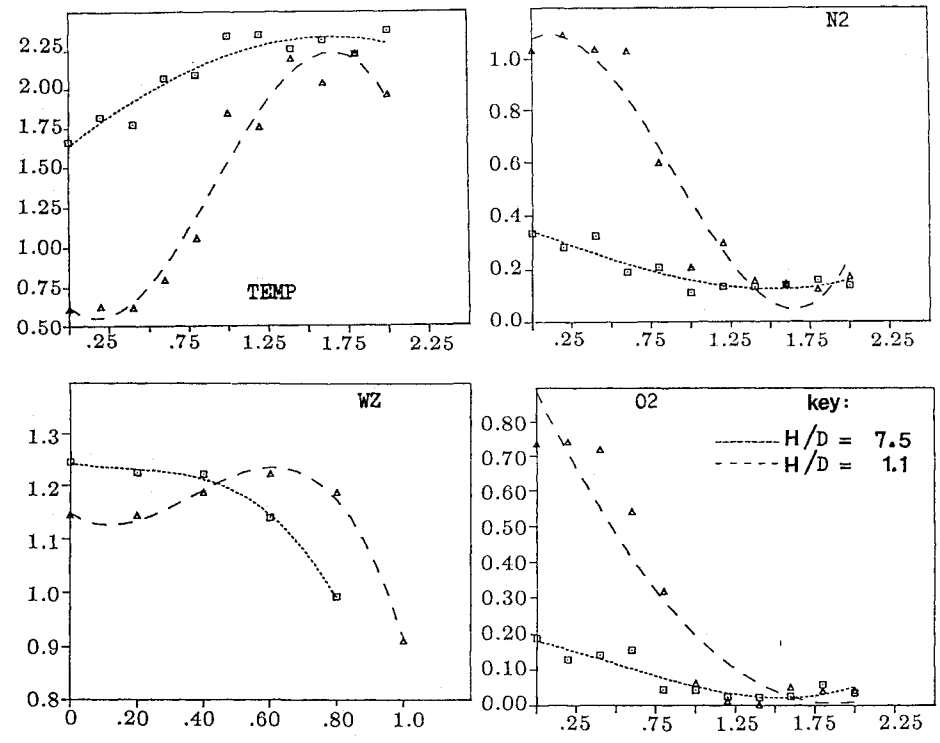

Fig. 9 Nozzle-stabilized impinging flame radial profiles: H/D = 1.1 and 7.5, Z/D = 0.2.

in value with $z'/D = \pm 2.0$. At once noticeable in Figs. 8a and 8b is the characteristic temperature profile of the free flame showing the local maximums at the flame core tip, flame core interface, and outer flame front, with the lowest temperature peak on the outer front in Fig. 8b and at the flame core tip in Fig. 8a. The interface and outer front maxima at $z'/D = 7.4$ appear less accentuated as one might expect near the vicinity of the postcore region where the reaction has diminished and temperatures reach their maxima. It is also interesting to note that the velocity values at $z'/D = 7.4$ do not drop off as quickly as at $z'/D = 7.1$ due to the elevated temperatures and subsequent gas expansion there. One can see that the hottest part of the flame with the largest temperature values is in the postcore region, while the coolest part is in the region above the nozzle prior to the core tip, with the N_2 and O_2 values responding accordingly and with the O_2 values being lower as expected and, in fact, going to zero on the centerline in the postcore region. The free flame plots provide a basic reference for the stagnation flows to follow.

Figure 2d visually shows the structure of the impinging nozzle-stabilized flame. In Figs. 9 and 10, the profiles show the behavior of the data with respect to the core tip position for two

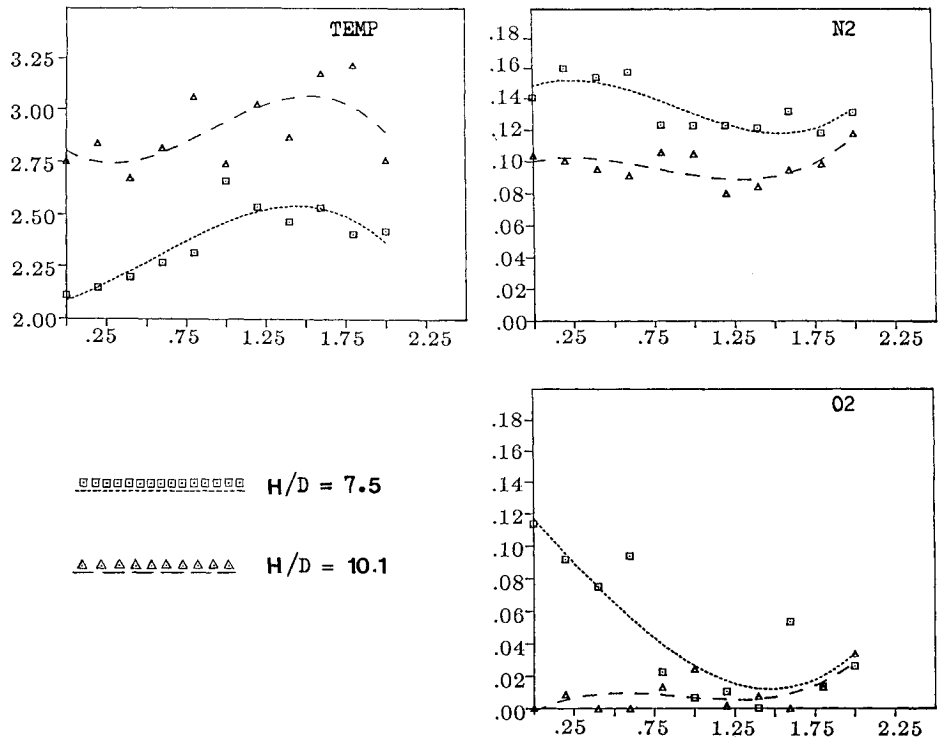

Fig. 10 Nozzle-stabilized impinging flame radial profiles: $H/D = 7.5$ and 10.1, $Z/D = 0.3$.

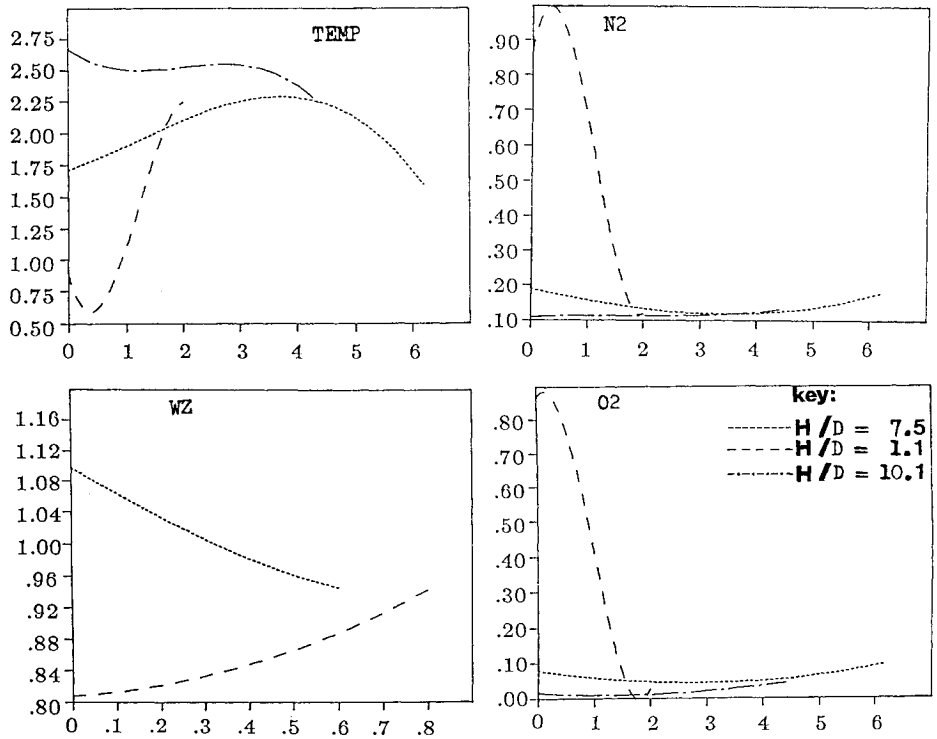

Fig. 11 Nozzle-stabilized impinging flame radial profiles: $H/D = 1.1$, 7.5, and 10.1; $Z/D = 0.1$.

values of z/D and show only moderately cooler temperatures and higher densities adjacent to the surface. The interesting point about Fig. 9 is that profiles for $H/D = 1.1$ display similar behavior to that in the free jet, with the higher centerline densities and velocities and cool temperatures gradually changing toward the flame front, but where the maximum temperature value is lower as expected; however, in the profiles at $H/D = 10.1$, the temperature profile reaches a higher maximum than that of the corresponding free flame profile of Fig. 8c. This result may be somewhat unexpected but, in light of the discussion by Law, straining a lean-mixture flow can cause elevated temperatures and under certain conditions could be responsible for the present results. The nature of the data for the $H/D = 10.1$ position indicates steady intermittent reaction zones due to the straining of the already low O_2 content mixture there. In general, the flame near the core tip and above undergoes the greatest change due to the presence of the plate.

In a similar fashion, the data taken at $z/D = 0.1$ for all three plate positions in the flame are plotted together in Fig. 11. The same basic tendencies that predominate in Figs. 9 and 10 also apply here; notice the overall core and postcore temperature values, however, are lower than in the previous figures and the

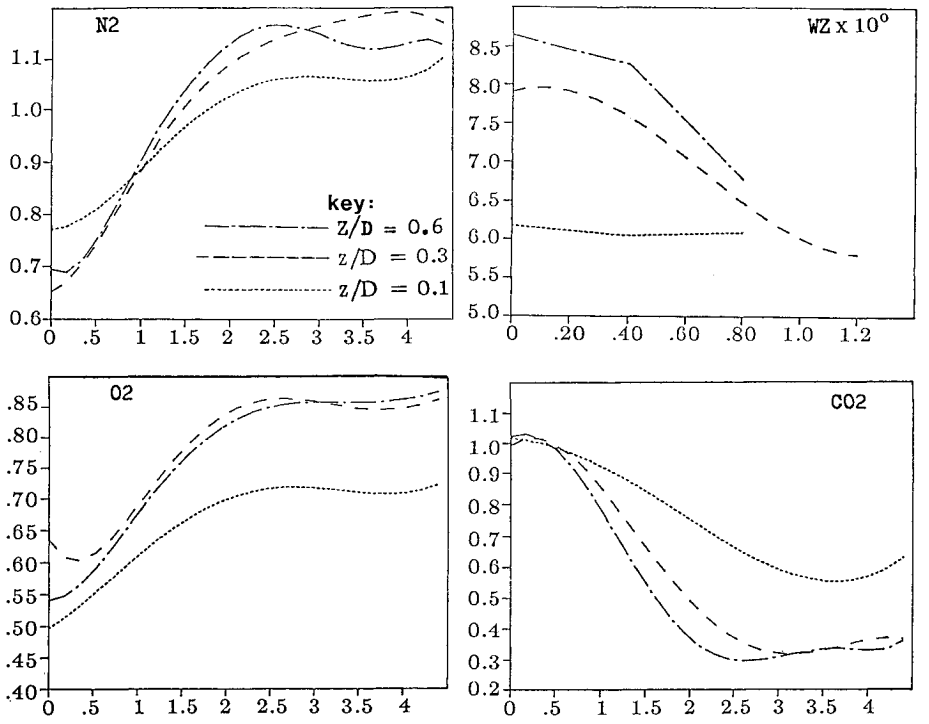

Fig. 12 Cold CO_2-air-CH_4 impinging jet radial profiles: $H/D = 3.1$; $Z/D = 0.1$, 0.3, and 0.6.

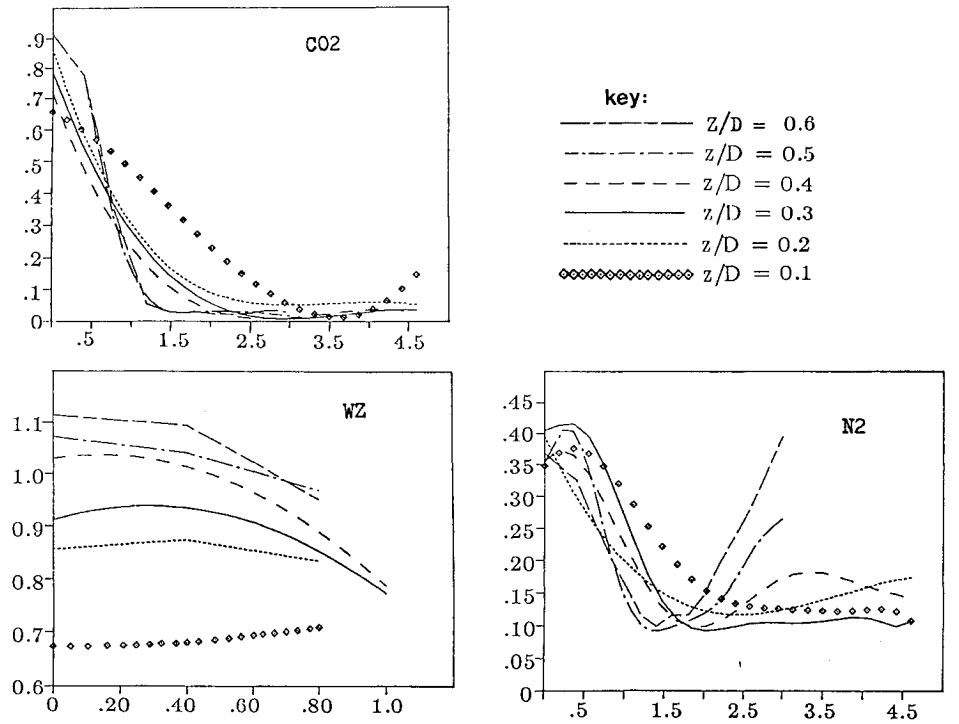

Fig. 13 Nozzle-stabilized reacting CO_2-air-CH_4 impinging flame radial profiles: $H/D = 3.1$, $Z/D = 0.1$-0.6.

density values of N_2 and O_2 are very similar, with the O_2 values only somewhat lower in this basically cool thermal boundary-type layer, which appears to be relatively thin, seemingly even thinner than that in the unattached flame measurements. Outside this layer, the reaction is moderately affected by the cooling of the plate.

Nozzle-Stabilized Flames with CO_2

This group of data is aimed at studying, through the use of cold CO_2 jets, the same geometrical stagnation flows with and without reaction occurring. For safety reasons, the cold jets had the amount of CH_4 reduced to six times lower than that in the reacting case; yet since by weight CH_4 was the smallest amount of reactant used in the flame, the nozzle velocities differ only slightly: $w_D = 10.2$ ft/s for the reacting case vs $w_D = 10.1$ ft/s for the cold jet. Due to this small difference in velocity and mass, it was felt the cold jet still retained much of the same initial momentum and diffusion properties of the reacting jet. The fuel-air ratio used had the value $F/A = 0.3728$, or $\phi = 1.3469$. It would be more appropriate to use a factor that accounts for the CO_2 presence, namely, a fuel/oxidant-inert ratio $F/OI = 0.26065$. Here again, $H/D = 3.1$.

The cold jet data involving the stagnation surface is shown in Fig. 12, which gives comparative results for the positions

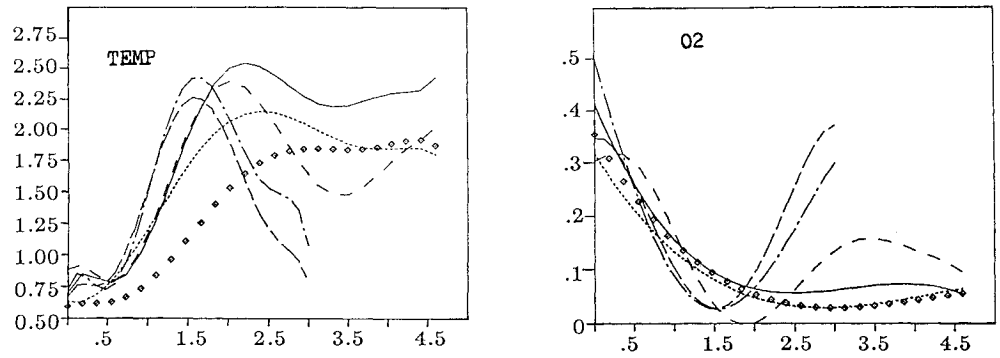

Fig. 13 Continued; nozzle-stabilized reacting CO_2-air-CH_4 impinging flame radial profiles.

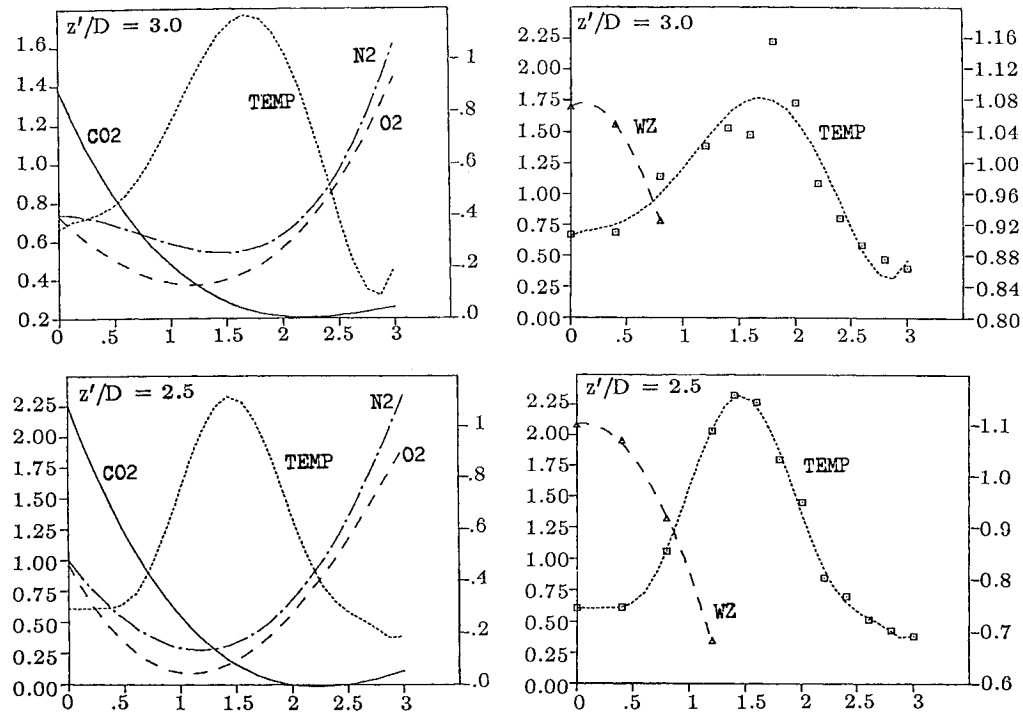

Fig. 14 Nozzle-stabilized reacting CO_2-air-CH_4 free flame radial profiles: Z'/D = 3.0 and 2.5 (temperature is the left ordinate).

z/D = 0.1, 0.3, and 0.6. Note that N_2 and O_2 density values are lowest at the centerline position because they are diluted by the CO_2 and then rise near the outer regions, where the CO_2 has become diffused; likewise, the CO_2 behaves in the contrary manner. It appears more CO_2 is entrained along the z/D = 0.1 region; therefore, the CO_2 levels diffuse more slowly there. The slight rise of some N_2 concentration values above 1.0 may be due to the cooling presence of the plate. There is another important note here: the O_2 concentration value is consistently below that of the N_2 value, despite the fact that there is no reaction taking place. This would seem to indicate that N_2 and O_2 have somewhat different diffusion properties (recalling that O_2 is heavier than N_2) in a N_2-O_2-CO_2 mixture, possibly causing O_2 to reach its ambient levels more slowly than N_2. This fact is important since these diffusion properties are likely to be affected by changes in temperature; this should be kept in mind when analyzing the reacting data to follow where the O_2 concentration will vary with its participation in the reaction as well. The w_z plot in this figure at z/D = 0.1 shows the expected drop in velocity values and the eventual "flattening" of the w_z curve. Yet only at about z/D = 0.3 does the centerline value of w_z drop to about half of its value at the nozzle. At z/D = 0.1, the CO_2 concentration levels stay surprisingly high—past r/R = 4.0; in a corresponding manner, O_2 and N_2 density levels stay somewhat lower, i.e., below their ambient levels, although N_2 density does so to a lesser extent. The presence of the plate has the overall effect of forming a thin boundary-type layer with sufficient momentum to extend relatively far along the radial positions and, in fact, may be the primary part of the wall jet region.

Figure 13 shows all of the profiles for the reacting case from z/D = 0.1–0.6 on a comparative basis. Note the cool temperature around the centerline where the CO_2 concentration is the greatest and the eventual temperature rise and subsequent N_2 and O_2 density decrease starting around r/R = 1.5. (Note: the diamond symbols in Fig. 13 are not data points—just curve-fit symbols.) Noting the temperature plot, a fascinating pattern develops: the temperature rises from its lowest value at z/D = 0.1 just adjacent to the plate to a maximum only 3 mm away at z/D = 0.3 where the maximum temperature value is actually higher than any value measured in the free jet as shown in Fig. 14. This temperature behavior is similarly reflected in the N_2 concentration profiles, where the profile at z/D = 0.3 yields the lowest concentration values, again lower than any measured in the corresponding free jet. For the positions z/D = 0.4–0.6, there is a decrease in overall temperature values, and the profiles revert to the characteristic shape of the free jet structure, with a sharper well-defined temperature maximum describing the lateral flame front and with the N_2, O_2, and CO_2 concentration profiles responding accordingly. A

similar response in the w_z plots cannot be accurately singled out since a temperature increase at $z/D = 0.3$ may not be large enough to reflect a substantial increase in w_z at that location due to its proximity to the plate. Suffice it to say that w_z measurements yield expected behavior in the vicinity of the plate, dropping off rapidly in the radial profile closest to the plate. Note for the profiles $z/D = 0.1$–0.3, the O_2 values show little or no difference in their overall behavior, most likely due to the aforementioned correlation with the presence of larger CO_2 concentration values nearer the plate and the associated diffusion mechanisms there.

Conclusions

It is quite clear from the data presented that the stagnation flowfield can and does affect the reaction process taking place to various degrees, especially via the process of blowing and the concept of flame stretch.

Some observations in summary follow.

Unattached Flames

Due to the nature of the flow, the flame front cannot be stabilized in a substantial straining region, and thus variations in blowing rates have no direct effect on the reaction and subsequent reaction-related temperature changes other than moving the apparent flame front to different radial positions, while changing its overall shape and being able to create a centrally cooler nonreacting region. Extreme strain causes complex "ring" flame structure requiring stability analysis.[17]

Because of the cooler central region of the flame structure and similarity to cold wall jet structure exhibited in limited measurements in the wall jet zone ($r/R \geq 1.8$), the problem may be partly amenable to theoretical treatment via modified cold boundary-layer and wall jet analysis.

Attached Flames

Here, behavior previously identified by Law in controlled, specialized, thin uniform flame geometries has been observed in simple typical multizone premixed flames subjected to a basic flow nonuniformity (i.e., velocity gradients found in stagnation flow) without variations in the blowing rates. The heat transfer to the stagnation surface is consistent with values previously observed for similar reacting cases.

Premixed CO_2 Flames

A quench zone along the plate, i.e., a region where reaction has been inhibited, has been observed via measurements of the premixed CO_2 data (and to a lesser extent, the previous two cases) to be quite thin (of the order ~ 1 mm) where both cold and reacting CO_2 data exhibit similar behavior. Reaction outside this zone appears to be rather vigorous, judging by temperature profiles there, and seems not to be greatly affected by the cooling effects of the wall. One can venture to hypothesize that this quench zone may even well approximate the boundary-layer thickness for the reacting flow. There are sources[13] that report relative insensitivity of flame extinction and quenching to the nature and temperature of the stagnation surface in similar reaction problems, which may lend support to this hypothesis. In any case, the thinness of the quench zone appears well based.

References

[1]Lapp, M., Penney, C. M., and Asher, J. A., "Application of Light-Scattering Techniques for Measurements of Density, Temperature and Velocity in Gasdynamics," Wright-Patterson Aerospace Research Labs., Wright-Patterson AFB, OH, Rept. ARL73-0045, April 1973.

[2]Tromans, P., "The Interaction Between Strain Fields and Flames—A Possible Source of Combustion Variations in Spark Ignition Engines," American Society of Mechanical Engineers, New York, June 1981.

[3]Lederman, S., "The Use of Laser Raman Diagnostics in Flow Fields and Combustion," *Progress in Energy and Combustion Science,* Vol. 3, Jan. 1977, pp. 1–34.

[4]Lederman, S., "Developments in Laser Based Diagnostic Techniques," *Proceedings of the 12th International Symposium on Shock Tubes and Waves,* edited by A. Lifshitz and J. Rom, Maguess Press, The Hebrew Univ., Jerusalem, Israel, 1980, pp. 48–65.

[5]Lederman, S. and Posillico, C. J., "Unified Spontaneous Raman and CARS System," *AIAA Journal,* Vol. 19, June 1981, pp. 824–825.

[6]Milson, A. and Chigier, N., "Studies of Methane and Methane-Air Flames Impinging on a Cold Plate," *Combustion and Flame,* Vol. 21, No. 3, 1973.

[7]Glauert, M. B., "The Wall Jet," *Journal of Fluid Mechanics,* Vol. 1, 1956.

[8]Martin, H., *Advances in Heat Transfer,* Vol. 13, edited by J. P. Hartnett and T. F. Irvine, Academic, New York, 1977.

[9]Bradshaw, P. and Love, M., "The Normal Impingement of a Circular Air Jet on a Flat Surface," British Aeronautical Research Council, R&M 3205, 1959.

[10]Law, C. K., "Heat and Mass Transfer in Combustion: Fundamental Concepts and Analytical Techniques," *Progress in Energy and Combustion Science,* Vol. 10, 1984, pp. 295–318.

[11]Buckmaster, J. D. and Ludford, G. S. S., *Theory of Laminar Flames,* Cambridge Univ. Press, London, 1982.

[12]Westbrook, C. K., Adamczyk, A., and Lavoie, G., "A Numerical Study of Laminar Flame Wall Quenching," *Combustion and Flame,* Vol. 40, 1981, pp. 81–89.

[13]Saitoh, T., "Extinction Analysis of Premixed Flame for Counter Flow and Blunt Body Forward Stagnation Region Flow," *International Journal of Heat and Mass Transfer,* Vol. 17, 1974, pp. 1063–1077.

[14]Karlovitz, B., Denniston, D., Knapschaefer, D., and Wells, F., "Studies on Turbulent Measurement in Flames," *Proceedings of the Fourth International Symposium on Combustion,* Williams and Wilkins, Baltimore, MD, 1953.

[15]Sato, J. and Tsuji, H., *Proceedings of the 16th Japanese Symposium on Combustion,* 1978, pp. 13–15.

[16]Posillico, C. J., "Raman Spectroscopic and LDV Measurements of a Methane Jet Impinging Normally on a Flat Water-Cooled Boundary," Ph.D. Dissertation, Polytechnic Univ., Farmingdale, NY, June 1986.

[17]Posillico, C. J. and Lederman, S., "Reacting Stagnation Flow," *Combustion and Flame* (to be published).